Iron robbery by intracellular pathogen via bacterial effector–induced ferritinophagy

Qi Yan[a], Wenqing Zhang[a], Mingqun Lin[a], Omid Teymournejad[a], Khemraj Budachetri[a], Jeffrey Lakritz[b], and Yasuko Rikihisa[a,1]

[a]Department of Veterinary Biosciences, The Ohio State University, Columbus, OH 43210; and [b]Department of Veterinary Preventive Medicine, The Ohio State University, Columbus, OH 43210

Contributed by Yasuko Rikihisa, April 30, 2021 (sent for review December 30, 2020; reviewed by Robert A. Heinzen and Daniel Voth)

Iron is essential for survival and proliferation of *Ehrlichia chaffeensis*, an obligatory intracellular bacterium that causes an emerging zoonosis, human monocytic ehrlichiosis. However, how *Ehrlichia* acquires iron in the host cells is poorly understood. Here, we found that native and recombinant (cloned into the *Ehrlichia* genome) *Ehrlichia* translocated factor-3 (Etf-3), a previously predicted effector of the *Ehrlichia* type IV secretion system (T4SS), is secreted into the host cell cytoplasm. Secreted Etf-3 directly bound ferritin light chain with high affinity and induced ferritinophagy by recruiting NCOA4, a cargo receptor that mediates ferritinophagy, a selective form of autophagy, and LC3, an autophagosome biogenesis protein. Etf-3–induced ferritinophagy caused ferritin degradation and significantly increased the labile cellular iron pool, which feeds *Ehrlichia*. Indeed, an increase in cellular ferritin by ferric ammonium citrate or overexpression of Etf-3 or NCOA4 enhanced *Ehrlichia* proliferation, whereas knockdown of Etf-3 in *Ehrlichia* via transfection with a plasmid encoding an Etf-3 antisense peptide nucleic acid inhibited *Ehrlichia* proliferation. Excessive ferritinophagy induces the generation of toxic reactive oxygen species (ROS), which could presumably kill both *Ehrlichia* and host cells. However, during *Ehrlichia* proliferation, we observed concomitant up-regulation of *Ehrlichia* Fe-superoxide dismutase, which is an integral component of *Ehrlichia* T4SS operon, and increased mitochondrial Mn-superoxide dismutase by cosecreted T4SS effector Etf-1. Consequently, despite enhanced ferritinophagy, cellular ROS levels were reduced in *Ehrlichia*-infected cells compared with uninfected cells. Thus, *Ehrlichia* safely robs host cell iron sequestered in ferritin. Etf-3 is a unique example of a bacterial protein that induces ferritinophagy to facilitate pathogen iron capture.

Ehrlichia chaffeensis | ferritinophagy | T4SS effector | iron | Etf-3

Ehrlichia spp., rickettsial obligatory intracellular bacteria cause tick-borne infectious diseases, which are greatly rising in worldwide prevalence (1, 2). *Ehrlichia chaffeensis* causes human monocytic ehrlichiosis, a severe flu-like illness accompanied by hematologic abnormalities and hepatitis, which can be fatal (2 to 5% mortality) (3–6). In humans, *E. chaffeensis* infects monocytes and macrophages and concocts unique membrane-bound compartments (inclusions). The inclusions have early endosome-like characteristics, including the presence of transferrin (Tf), transferrin receptor (TfR), and vacuolar-type H^+-ATPase as well as the small GTPase RAB5 and its effectors, but the inclusions lack late endosomal or lysosomal markers or NADPH oxidase (7–9). Within the inclusions, *Ehrlichia* acquires all nutrients, including iron, for its reproduction to yield numerous mature infectious forms.

Iron serves as a cofactor in many processes of bacteria and eukaryotes, including electron transfer, energy metabolism, oxygen transport, oxygen sensing, and DNA synthesis and repair (10). *Ehrlichia* is an obligate aerobe and is absolutely dependent on host iron for ATP synthesis via the electron transport chain, because its glycolytic pathway is incomplete and it lacks ATP–ADP translocase, unlike *Rickettsia* and *Chlamydia* (11). *E. chaffeensis* lacks the siderophore biosynthesis pathway and Fe^{3+} uptake regulator (11). Nonetheless, *Ehrlichia* acquires iron from the host cell labile cellular iron (LCI) pool, and pretreating human monocytes with the membrane-permeable iron chelator deferoxamine blocks *E. chaffeensis* infection (12). *Ehrlichia* enhances host cell iron uptake via up-regulating TfR messenger RNA (mRNA) (13) and acquires iron from the holoTf, as *E. chaffeensis* endosomes intersect with TfR-recycling endosomes and are slightly acidic—enough to release iron from holoTf (7). In fact, treatment of macrophages with interferon-γ down-regulates TfR mRNA and almost completely inhibits *Ehrlichia* infection, and addition of holoTf abrogates this inhibition (12). However, TfR mRNA levels return to basal level after 24 h postinfection when bacterial exponential growth begins (13), and treatment with interferon-γ can no longer inhibit infection at this point (12), suggesting that alternative or additional iron acquisition mechanisms exist to support exponential intracellular growth of *Ehrlichia*.

The bacterial type IV secretion system (T4SS) translocates bacterial proteins and nucleoprotein complexes (called "effectors," as they bring about responses) from bacteria to eukaryotic cells (14). Rickettsial organisms including *E. chaffeensis* have T4SS, sometimes referred to as T4aSS, similar to the *virB/virD* system of *Agrobacterium tumefaciens* (15, 16). The *dot/icm* system of *Legionella pneumophila*, sometimes referred to as T4bSS, secretes ∼300 effectors with redundant functions; hence, each effector can be knocked out, but the mutant lacks a phenotype (17). In contrast, the total number of T4aSS effectors is much lower [for example, fewer than six effectors exist in *A. tumefaciens* (15)], but

Significance

***Ehrlichia chaffeensis* infects and proliferates inside monocytes and macrophages by acquiring iron from the cellular labile iron pool and causes a potentially fatal disease called human monocytic ehrlichiosis. This report reveals a unique bacterial iron hijacking mechanism. *Ehrlichia* deploys a protein Etf-3 via the bacteria type IV secretion system. Etf-3 binds ferritin and induces ferritinophagy, thereby increasing the cellular labile iron pool for *Ehrlichia* to acquire iron for intracellular proliferation. This, in concert with coregulation of bacterial and host cell superoxide dismutases with type IV secretion system, enables *Ehrlichia* to prevent reactive oxygen species–induced host cell damage mediated by labile iron. This finding unifies current concepts of intracellular bacterial infection, ferritinophagy, and ROS, which may be exploited to inhibit *Ehrlichia* infection.**

Author contributions: Q.Y. and Y.R. designed research; Q.Y., W.Z., O.T., K.B., and J.L. performed research; Q.Y., W.Z., M.L., and Y.R. analyzed data; and Y.R. wrote the paper.

Reviewers: R.A.H., Rocky Mountain Laboratories; and D.V., University of Arkansas for Medical Sciences.

The authors declare no competing interest.

[1]To whom correspondence may be addressed. Email: rikihisa.1@osu.edu.

This article contains supporting information online at https://www.pnas.org/lookup/suppl/doi:10.1073/pnas.2026598118/-/DCSupplemental.

Published May 31, 2021.

each effector has a crucial role in infection/disease. To date, only a handful of T4SS effectors have been identified for rickettsial organisms, and even fewer have been functionally characterized (18–21). VirD4 is a well-established coupling protein involved in escorting translocated DNA and proteins in *A. tumefaciens* (15). By a bacterial two-hybrid screen using *E. chaffeensis* VirD4 as bait, we previously identified three *Ehrlichia* proteins that directly bind to *Ehrlichia* VirD4: ECH0825 (Ehrlichial translocated factor-1, Etf-1), ECH0261 (Etf-2), and ECH0767 (Etf-3) (22). All three were formerly annotated as hypothetical proteins, as they lack sequence similarity to previously known proteins or protein domains or motifs. Etf-1 has key roles in *Ehrlichia* infection of human cells by blocking host cell apoptosis and inducing RAB5-regulated autophagy for nutrient (amino acids) acquisition (9, 22, 23). Etf-2 is a unique RABGAP5 structural mimic that lacks GTPase-activating protein activity (24). Etf-2 directly binds RAB5-GTP on the *Ehrlichia* inclusion membrane and impedes the fusion of *Ehrlichia*-containing early endosomes with lysosomes (24). Whether Etf-3 is secreted or has any biological function is unknown. In the present study, we discovered that Etf-3 is a true T4SS effector that is secreted, binds tightly to ferritin, and induces ferritinophagy to provide free Fe^{2+} for intracellular *Ehrlichia*.

Results

Native Etf-3 and FLAG-Etf-3, but Not FLAG-Etf-3ΔC, Are Secreted from *Ehrlichia* and Localize in Puncta within the Host Cell Cytoplasm. Etf-3 (621 amino acid residues, 70,523 Da) is highly conserved (99 to 100% amino acid sequence identity) among eight *E. chaffeensis* strains, which were isolated via culture of blood samples from patients with monocytic ehrlichiosis in five different states in the United States during the period 1991–1998 and for which whole-genome sequences have been determined (*SI Appendix*, Fig. S1). This suggested that the functions of Etf-3 are essential for the survival of *E. chaffeensis* (25). Also, Etf-3 mRNA/protein is expressed by *E. chaffeensis* in the human acute monocytic leukemia cell line THP-1 (22), human promyelocytic leukemia cell line HL-60 (26), canine histiocytic leukemia cell line DH82, and tick embryonic cell line ISE6 (National Center for Biotechnology Information Gene Expression Omnibus [GEO] accession #GSE56339) (27). Immunofluorescence labeling with anti–Etf-3 revealed that native *E. chaffeensis* Etf-3 could be clearly detected in distinct puncta within the host cell cytoplasm (Fig. 1*A*). Effector secretion analysis is not possible using the autologous T4SS for obligatory intracellular bacteria, which include all members of the order Rickettsiales, as conventional bacterial genetics systems are not available for these bacteria (28). *A. tumefaciens* T4S substrates consensus secretory motif R-X(7)-R-X-R-X-R-X-X(n), where Arg can be replaced with Lys with negligible effect, is located in the C terminus (29). Therefore, to confirm Etf-3 secretion and analyze the secretory motif, we used the Himar1 transposon random mutagenesis system (30) to insert a gene encoding FLAG-Etf-3 or FLAG-Etf-3ΔC ([residues 1 to 588 or $AA^{1\text{-}588}$] into the *E. chaffeensis* chromosome and assessed FLAG-Etf-3 and FLAG-Etf-3ΔC secretion. We found that, although both FLAG-Etf-3 and FLAG-Etf-3ΔC were expressed by *E. chaffeensis*, only FLAG-Etf-3 was translocated to the cytoplasm of infected cells, indicating that the Etf-3 C-terminal secretion signal is required for translocation across three membranes, that is, the bacterial inner and outer membranes and host cell inclusion membrane (Fig. 1 *B* and *C*). The secreted FLAG-Etf-3 formed numerous puncta in the cytoplasm of infected cells as native Etf-1 (Fig. 1*A*), suggesting Etf-3 associates with the host cytosolic macromolecular protein complex and/or intracellular vesicles. Moreover, intracellular growth of FLAG-Etf-3–transformed *E. chaffeensis* is significantly greater than wild-type *E. chaffeensis* (*SI Appendix*, Fig. S2).

Etf-3 Enhances *E. chaffeensis* Infection, and an Etf-3–Specific Antisense Peptide Nucleic Acid Inhibits Infection. We used qRT-PCR for the *Ehrlichia* 16S ribosomal RNA (rRNA) to examine whether Etf-3 overexpression affects *Ehrlichia* infection. Compared with GFP-overexpressing control cells, Etf-3-GFP overexpression significantly enhanced *Ehrlichia* infection (Fig. 2*A*). No Etf-3 deletion mutants are currently available, because classical bacteriology techniques such as targeted mutagenesis are not readily applicable for obligatory intracellular bacteria, and, unlike facultative intracellular bacteria, knockout mutants for genes essential for intracellular infection (e.g., Etf-3) cannot be recovered (28). Peptide nucleic acid (PNA) is a DNA mimic that has been shown to bind single- and double-stranded DNA and RNA with high affinity (higher than DNA itself) and specificity (31), and inhibit transcription from double-stranded DNA (32, 33) and translation (34, 35). Therefore, we designed an antisense PNA that specifically binds near the translation start site of Etf-3 (Fig. 2 *B–D*). Electroporation of purified *Ehrlichia* with this PNA significantly reduced Etf-3 mRNA expression (Fig. 2*E*), and intracellular replication

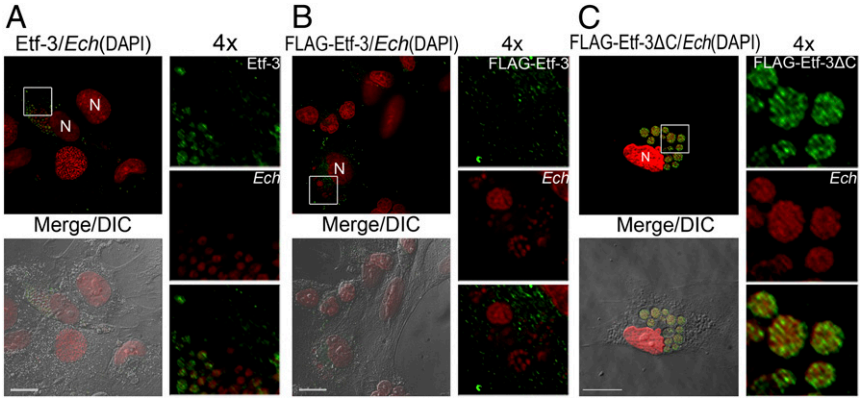

Fig. 1. Native *Ehrlichia* Etf-3 and FLAG-tagged Etf-3 or Etf-3ΔC cloned into the *Ehrlichia* genome were expressed, and Etf-3 and FLAG-tagged Etf-3 were secreted into the host cell cytoplasm and appeared as puncta, but FLAG-tagged Etf-3ΔC was not secreted. (*A*) *E. chaffeensis* (*Ech*)-infected RF/6A cells at 2 days post-infection (dpi) were fixed and labeled with llama anti-Etf-3 IgG and AF488-anti-llama IgG. (*B* and *C*) The pCis-FLAG-Etf-3-SS-Himar A7 (*B*) or pCis-FLAG-Etf-3ΔC-SS-Himar A7 plasmid (*C*) encoding FLAG-tagged Etf-3 or Etf-3ΔC was transformed into *Ehrlichia* and used to infect RF/6A cells. Cells at 2 dpi were fixed and labeled with AF488-rat anti-FLAG monoclonal antibody. Bacteria (*Ech*) and the host cell nucleus (N) were labeled with DAPI (pseudocolored red). Native *Ehrlichia* Etf-3 (*A*), and FLAG-tagged Etf-3 (*B*) and Etf-3ΔC (*C*), were expressed, but only native Etf-3 and FLAG-tagged Etf-3 were secreted, forming puncta in the cytoplasm of infected RF/6A cells. DIC, differential interference contrast; Merge/DIC, merge of the fluorescence and DIC images. Each boxed area is enlarged 4× on the right. (Scale bars: 10 μm.)

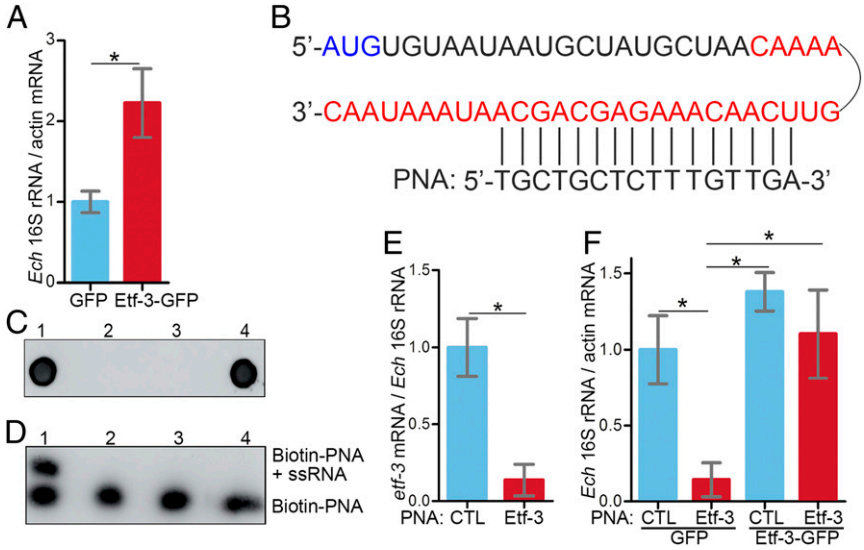

Fig. 2. Overexpression of Etf-3 promotes *Ehrlichia* infection, and *etf-3*–specific antisense PNA inhibits *Ehrlichia* infection. (*A*) HEK293 cells were transfected with a plasmid encoding Etf-3-GFP or GFP for 16 h, and infected with freshly purified *E. chaffeensis* for 2 d. Bacterial numbers in each sample were determined by qRT-PCR using specific primers for *Ehrlichia* 16S rRNA and were normalized against the level of human actin mRNA. Data are presented as the mean ± SD from three independent experiments. Asterisk (*): Significantly different by Student's *t* test ($P < 0.05$). (*B–D*) Etf-3 PNA knocks down *Ehrlichia etf-3* mRNA expression and decreases *E. chaffeensis* proliferation. (*B*) Etf-3 PNA targets the *etf-3* mRNA. The mRNA sequence of *etf-3* from the translational start site (AUG) is shown on the top, and the Etf-3 single-stranded RNA (ssRNA) sequence designed for the hybridization assay is shown in red. (*C*) Dot blot confirmation of biotinylation of PNAs using HRP-conjugated streptavidin. Dots 1 to 4: 1, biotin–Etf-3 PNA; 2, unlabeled Etf-3 PNA; 3, unlabeled control (CTL) PNA; 4, biotin–CTL PNA. (*D*) Electrophoretic mobility shift assay of biotinylated Etf-3 PNA bound to Etf-3 ssRNA. Lanes 1 to 4: 1, biotin–Etf-3 PNA incubated with Etf-3 ssRNA; 2, biotin–Etf-3 PNA only; 3, biotin–CTL PNA incubated with Etf-3 ssRNA; 4, biotin–CTL PNA only. (*E*) Etf-3 PNA significantly reduces *Ehrlichia etf-3* mRNA expression. HEK293 cells infected with Etf-3 PNA- or CTL PNA-transformed *E. chaffeensis* were harvested at 2 dpi and subjected to qRT-PCR analysis. The values reflect bacterial *etf-3* mRNA normalized against *Ehrlichia* 16S rRNA. (*F*) HEK293 cells expressing Etf-3 complement the Etf-3 PNA knockdown of *Ehrlichia* infection. HEK293 cells were transfected with Etf-3-GFP or GFP, and infected with Etf-3 PNA- or CTL PNA-transfected *Ehrlichia* at 1 day post-transfection (dpt). RNA samples were prepared at 2 dpi and subjected to qRT-PCR analysis. The values reflect bacterial 16S rRNA normalized against human actin mRNA. Data indicate the mean ± SD from three independent experiments that had three replicates per sample. Asterisk (*): Significantly different by Student's *t* test or ANOVA ($P < 0.05$).

(Fig. 2*F*). However, Etf-3 PNA did not affect *Ehrlichia* binding or entry into the host cells (*SI Appendix*, Fig. S3). Etf-3 PNA-mediated inhibition of Etf-3 expression and *Ehrlichia* replication could be reversed by ectopic expression of Etf-3-GFP in host cells (Fig. 2*F*). These results indicated the Etf-3 is critical for *Ehrlichia* replication in host cells.

Etf-3 Binds to Ferritin via Ferritin Light Chain at High Affinity. To identify host cell proteins that could bind to secreted Etf-3, Etf-3 was cloned into the bait vector of a yeast two-hybrid system, which was then used to screen a human leukocyte complementary DNA (cDNA) prey library. Sequencing of the prey plasmids isolated from stringent quadruple dropout plates revealed predominantly *Homo sapiens* ferritin light chain (FTL) (Fig. 3*A*). Ferritin is a protein complex composed of 24 subunits of FTL and ferritin heavy chains (FTH1). Ferritin can chelate up to 4,500 Fe^{3+} atoms (36). Etf-3 selectively bound FTL, but not FTH1, in the yeast two-hybrid system (Fig. 3*B*). Far-Western blotting (far-WB) confirmed that recombinant Etf-3 (rEtf-3), but not rEtf-1 (negative control), renatured on a polyvinylidene difluoride (PVDF) membrane could bind to iron-saturated native human holoferritin, implying that rEtf-3 binds to FTL exposed on the surface of holoferritin (Fig. 3*C*). Furthermore, immunoprecipitation of Etf-3-GFP–transfected or GFP-transfected (negative control) HEK293 cells revealed that endogenous FTL (ferritin) could be pulled down by Etf-3-GFP but not by GFP (Fig. 3*D*). Immunoprecipitation of *E. chaffeensis*-infected THP-1 cells also resulted in the pull-down of endogenous FTL (ferritin) by *Ehrlichia* native Etf-3 (Fig. 3*E*). OpenSPR (surface plasmon resonance) analysis revealed that rEtf-3 could bind to human holoferritin with high affinity (K_D = 5 nM) (Fig. 3*F*), but did not bind to rFTH1 (*SI Appendix*, Fig. S4).

Ectopically Expressed Etf-3 Colocalizes with Ferritin and Causes a Posttranscriptional Reduction of Ferritin. In Etf-3-GFP–transfected cells, Etf-3-GFP localized in distinct puncta (Fig. 4*A*), similar to what was observed for native Etf-3 and rEtf-3 that were secreted from *E. chaffeensis* (Fig. 1). Given that Etf-3 was secreted from *E. chaffeensis* into the host cell cytoplasm and bound FTL and ferritin with high affinity, we examined whether Etf-3-GFP ectopically expressed in mammalian cells could colocalize with endogenous ferritin using anti-FTL IgG or red fluorescent protein (RFP)-FTL in cotransfected cells. In Etf-3-GFP–transfected cells, Etf-3-GFP colocalized with ferritin or RFP-FTL, which also localized in puncta (Fig. 4 *A*, *C*, and *E*). Ectopic expression of GFP-Etf-1 induces Rab5-regulated autophagy, thus intracelluar puncta (9). In negative-control Etf-1-GFP–transfected or GFP-transfected cells, however, most ferritin or RFP-FTL was diffused in the cytoplasm and seldom localized in puncta (Fig. 4 *B* and *D* and *SI Appendix*, Fig. S5). WB revealed that the levels of endogenous FTL and FTH1 were significantly reduced in Etf-3-GFP–transfected cells compared with GFP-transfected cells (Fig. 4 *F* and *G*). The cellular ferritin level is also regulated at the transcriptional level (37). However, both FTL and FTH1 mRNA levels were not reduced in Etf-3-GFP–transfected cells compared with GFP-transfected cells (Fig. 4 *H* and *I*), indicating that Etf-3-GFP induced a posttranscriptional reduction of FTL.

Etf-3-GFP Colocalizes with the Autophagosome Biogenesis Protein LC3-II and Induces Ferritinophagy. Iron is incorporated into ferritin as Fe^{2+} via ferritin iron pores and then is oxidized to Fe^{3+} by FTH1 (ferroxidase) inside the ferritin cage, leading to inert Fe^{3+} deposits that are unavailable for intracellular use or reactive oxygen species (ROS) generation (38). Iron must be released

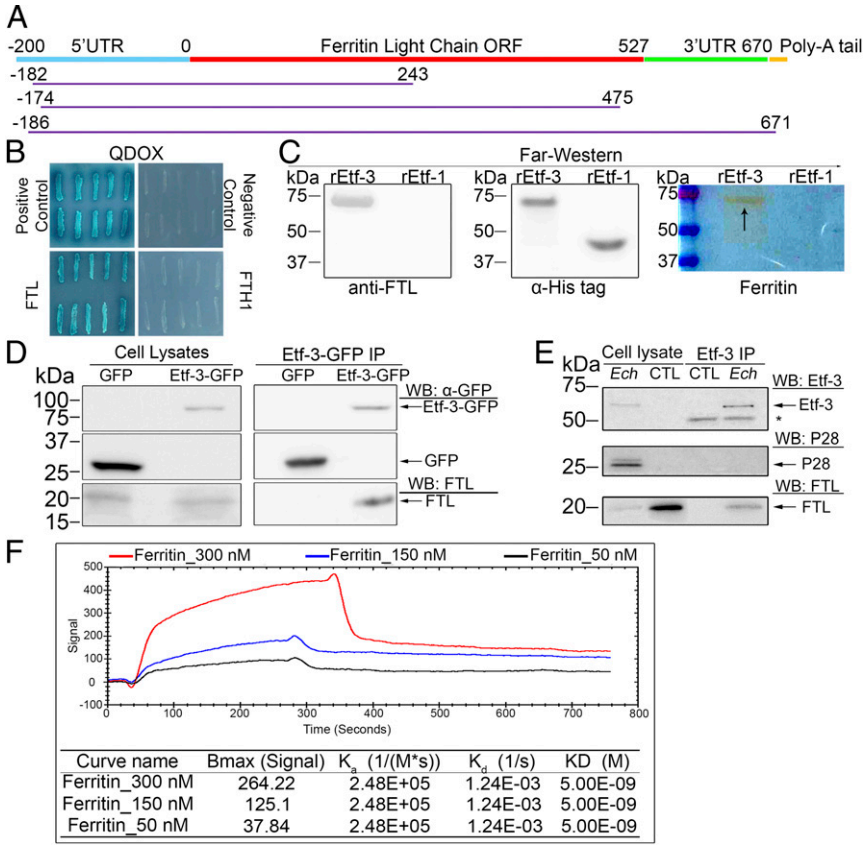

Curve name	Bmax (Signal)	K_a (1/(M*s))	K_d (1/s)	KD (M)
Ferritin_300 nM	264.22	2.48E+05	1.24E-03	5.00E-09
Ferritin_150 nM	125.1	2.48E+05	1.24E-03	5.00E-09
Ferritin_50 nM	37.84	2.48E+05	1.24E-03	5.00E-09

Fig. 3. Etf-3 directly binds to FTL. (*A*) Alignment of FTL sequences obtained from yeast two-hybrid screening (Y2H) with the human FTL full-length mRNA sequence. The blue line indicates the 5′ untranslated region (5′-UTR) of human FTL, the red line indicates the coding sequence, and the green line indicates the 3′-UTR. Full-length Etf-3 was used as the bait, and Human Leukocyte cDNA Library was used as the prey library. Examples of three distinct yeast clones (purple lines show FTL sequences) obtained from Y2H are shown. (*B*) Direct interaction of Etf-3 with FTL was confirmed using Y2H. Etf-3 was used as the bait, and FTL or FTH1 was used as the prey. The positive-control bait–prey pair was P53 and T antigen from the Matchmaker Gold Yeast Two-Hybrid System. The negative-control bait–prey pair was Etf-3 and $RAB5^{S/N}$. Ten independent diploid colonies were tested on SD/–Leu/–Trp/–His/–Ade –X-α-Gal quadruple-dropout (QDOX) agar plates. Growth and blue colonies on QDOX plates indicated a specific interaction between Etf-3 and FTL, but not FTH1. (*C*) Far-WB of renatured rEtf-3 and rEtf-1 on a PVDF membrane incubated with purified human holoferritin. Ferritin was detected with native brown color (arrow on *Right*) on the membrane and confirmed by anti-FTL, and recombinant proteins were detected with anti-histidine-tag (α-His tag). (*D* and *E*) Immunoprecipitation (IP) of endogenous ferritin with Etf-3-GFP–transfected or GFP-transfected HEK293 cells by anti-GFP affinity nanobody gel (*D*) and native Etf-3 with endogenous ferritin in *Ehrlichia* (*Ech*)-infected and uninfected (CTL) THP-1 cells with anti-Etf-3–coated protein A agarose (*E*). Results were analyzed with WB with anti-GFP, anti-FTL, anti-Etf-3, and/or anti-P28. The asterisk (*) indicates the IgG heavy chain. (*F*) Analysis of the binding kinetics of rEtf-3 with purified human ferritin via OpenSPR. Each curve corresponds to the responses of different ferritin concentrations (300, 150, or 50 nM), and all curves were corrected for the control curve. The dissociation constant of rEtf-3 for ferritin is 5 nM.

from ferritin and reduced back to Fe^{2+} for utilization via shuttling of ironbound ferritin to the lysosome, a process termed ferritinophagy (a form of selective autophagy) (39). Double-membrane vesicles called autophagosomes carry cellular components within an inner autophagic membrane, and fuse with lysosomes, liberating the autophagic body and its contents into the vacuolar lumen for degradation by a complex process involving at least 16 autophagy-related/ATG proteins. Among these, MAP1LC3/LC3 (microtubule-associated protein 1 light chain 3; a mammalian ortholog family of yeast ATG8), is the only ATG protein known to form a stable association with the membrane of autophagosomes which appear as puncta in the cytoplasm (40, 41). LC3 exists in two forms: cytosolic LC3-I and LC3-II, which is membrane-bound and is converted from LC3-I to initiate formation and lengthening of the autophagosome (40). Given the colocalization of Etf-3 and ferritin in cellular puncta and the significant reduction of ferritin in Etf-3–transfected cells, we examined whether Etf-3 colocalizes with LC3. Indeed, in Etf-3-GFP and RFP-LC3 cotransfected cells, Etf-3-GFP colocalized with RFP-LC3-II in puncta and with endogenous ferritin (Fig. 5 *A* and *C*), whereas, in GFP and RFP-LC3 cotransfected cells, LC3 did not form puncta, and endogenous ferritin neither formed puncta nor colocalized with RFP-LC3 or GFP (Fig. 5 *B* and *C*).

Since LC3 colocalized with Etf-3-GFP and FTL/ferritin, we used WB to examine whether ferritin and Etf-3-GFP were degraded by ferritinophagy. Endogenous ferritin (detected with anti-FTL) and Etf-3-GFP were significantly more degraded in Etf-3-GFP–transfected cells than in GFP-transfected cells, and treatment with the autophagy inducer rapamycin (42) enhanced degradation of ferritin and Etf-3-GFP in Etf-3-GFP–transfected cells, but not in GFP-transfected cells (Fig. 6 *A*–*C*). Treatment with the autophagy inhibitor 3-MA (3 methyl adenine) that inhibits class III PI3 kinase (43) or with the lysosomal cysteine protease cathepsin B inhibitor E64D (44) prevented the degradation of both ferritin and Etf-3-GFP (Fig. 6 *A*–*C*). LC3-II in the forming phagophore interacts with adaptor proteins to engulf autophagy cargo and eventually forms autolysosome, where cellular components and LC3-II in the autolysosomal lumen are degraded (45). LC3-II differs from LC3-I by its smaller size and covalent modification with lipid extensions (46). Owing to its principal role in autophagy, analysis of membrane-associated LC3-II levels has proven to be an efficient way to monitor autophagy. The ratio of endogenous LC3-II to LC3-I

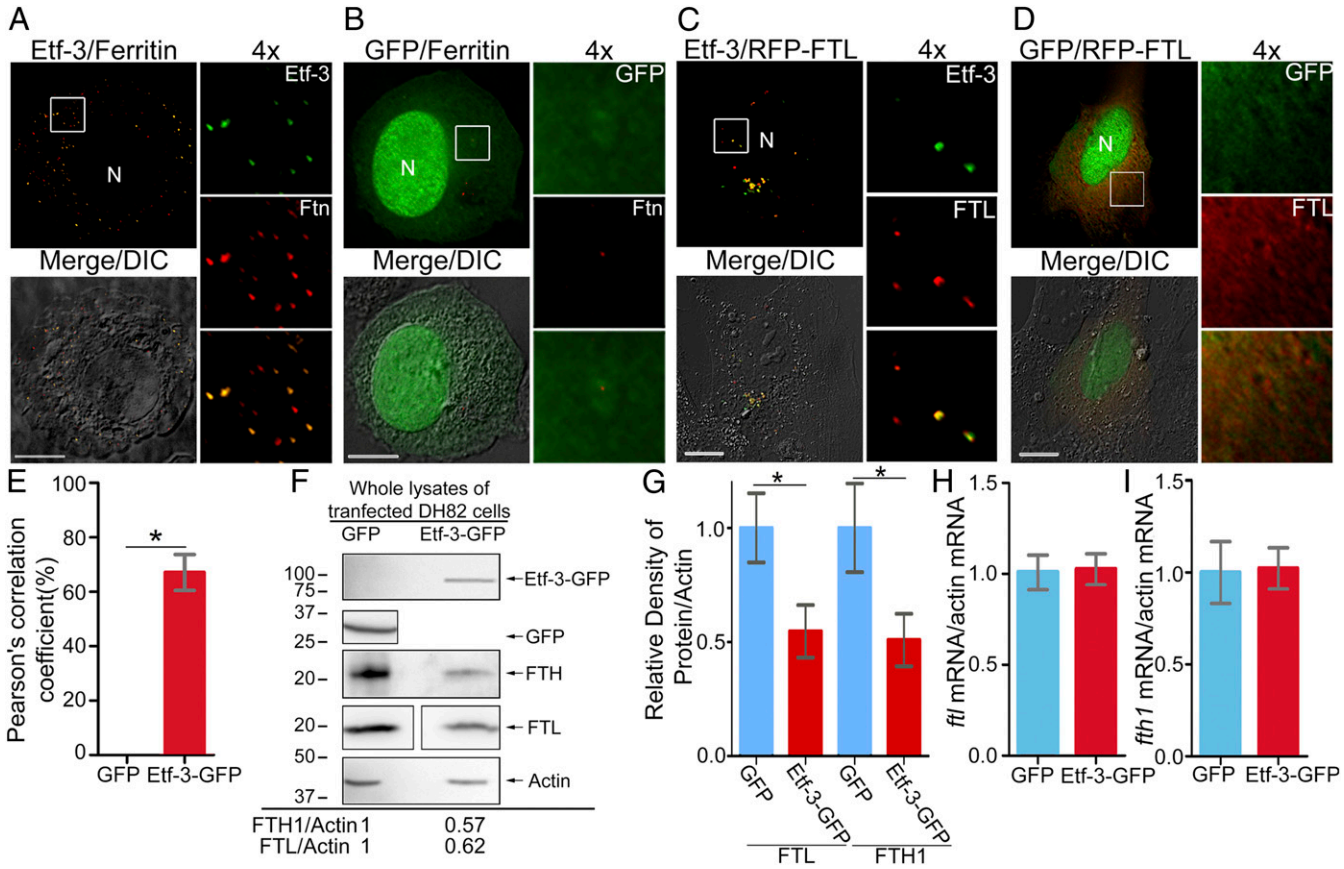

Fig. 4. Ectopically expressed Etf-3 colocalizes with endogenous ferritin and decreases ferritin, but not ferritin mRNA. (*A* and *B*) Ectopically expressed Etf-3 localizes to endogenous ferritin in a punctate pattern. DH82 cells were transfected with a plasmid encoding Etf-3-GFP (*A*) or GFP (control) (*B*). Ferritin was detected with anti-FTL. (*C* and *D*) Ectopically expressed Etf-3 colocalizes with RFP-FTL in RF/6A cells. Ftn, ferritin. Each boxed area is enlarged 4× on the right. (Scale bars: 10 μm.) (*E*) Colocalization of RFP-FTL with Etf-3-GFP or GFP was analyzed using Pearson's correlation coefficient. Asterisk (*): Significantly different by Student's *t* test ($P < 0.01$). (*F* and *G*) Ectopic expression of Etf-3 decreases endogenous ferritin protein amount. (*F*) DH82 cells were transfected with a plasmid encoding Etf-3-GFP or GFP. Transfected cells were harvested at 2 dpt for WB using anti-GFP, actin, FTH1, and FTL. (*G*) The relative band density of ferritin (FTH1 and FTL) was normalized against human actin. Endogenous ferritin (FTH1 and FTL) in Etf-3-GFP–transfected cells was decreased significantly compared with GFP-transfected cells. (*H* and *I*) Ectopic expression of Etf-3 does not alter ferritin mRNA expression. HEK293 cells were transfected with a plasmid encoding Etf-3-GFP or GFP, and qRT-PCR was performed at 2 dpt. The values reflect FTL (*H*) and FTH1 (*I*) mRNA normalized against human actin mRNA. For *G*–*I*, data indicate the mean ± SD from three independent experiments that had three replicates per sample. GFP control group was arbitrarily set to 1. Asterisk (*): Significantly different by Student's *t* test ($P < 0.05$).

was similar in Etf-3-GFP–transfected cells and GFP-transfected cells in the absence or presence of rapamycin, E64D, or 3-MA (Fig. 6 *A* and *D*), indicating that Etf-3 did not induce generalized autophagy although it led to the degradation of endogenous FTL/ferritin, implying the selective autophagy, ferritinophagy.

Etf-3 Facilitates the Interaction between Nuclear Receptor Coactivator 4 and Ferritin. When cells are treated with ferric ammonium citrate (FAC) that increases cellular ferritin, cytosolic protein nuclear receptor coactivator 4 (NCOA4) directly binds to FTH1 and LC3 and selectively mediates ferritinophagy (47). Thus, we examined whether NCOA4 is involved in ferritinophagy induced by Etf-3. In Etf-3-GFP and hemagglutinin (HA)-NCOA4 cotransfected cells, NCOA4 formed distinct puncta which colocalized with Etf-3-GFP puncta (Fig. 7 *A* and *D*). As controls, in GFP and HA-NCOA4 cotransfected cells, FAC treatment induced distinct puncta of NCOA4 (Fig. 7*B*), whereas, without FAC treatment, NCOA4 puncta were undetectable (Fig. 7*C*). In these cotransfected cells, GFP remained diffuse in the cytoplasm and did not make puncta, or colocalized with NCOA4 regardless of FAC treatment (Fig. 7 *B*–*D*). Moreover, when cells were cotransfected with HA-NCOA4 and Etf-3-GFP (or GFP, negative control), immunoprecipitation with anti-HA revealed significantly enhanced binding of ferritin (both FTH1 and FTL) to NCOA4 compared with only weak binding of endogenous FTH1 and FTL in GFP- or sham-transfected cells (Fig. 7 *E* and *F* and *SI Appendix*, Fig. S6). This indicated that Etf-3 binding to FTL in the ferritin complex induced NCOA4-mediated ferritinophagy. Further, NCOA4 overexpression significantly enhanced *Ehrlichia* infection (Fig. 7*G*).

Etf-3 Increases the LCI Pool via Ferritinophagy. To determine whether Etf-3–induced ferritinophagy indeed increases the LCI pool, intracellular Fe^{2+} level was determined with BioTracker 575 Red Fe^{2+} dye in live cells (48). In Etf-3-GFP–transfected cells, the LCI pool (intracellular Fe^{2+}) increased significantly compared with that in GFP-transfected cells (Fig. 8). This Etf-3-GFP–induced increase in the cellular LCI pool by Etf-3-GFP was blocked by 3-MA (Fig. 8 *D* and *E*), indicating that Etf-3-GFP–induced ferritinophagy increased the LCI pool.

***Ehrlichia* Infection Induces Degradation of Ferritin, Thereby Significantly Enhancing *Ehrlichia* Infection.** Because ectopic expression of Etf-3 induced ferritinophagy, we examined whether *Ehrlichia* infection could induce the degradation of host cell ferritin and assessed the

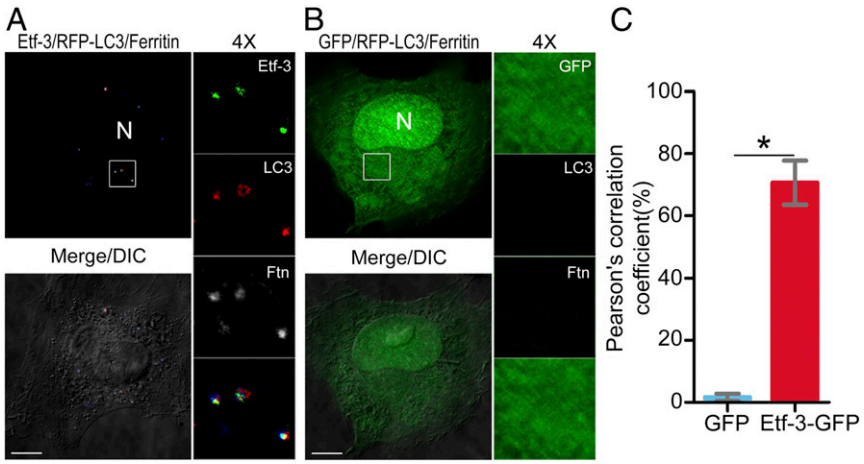

Fig. 5. Ferritin colocalizes with RFP-LC3 in the presence of Etf-3-GFP. (*A* and *B*) Endogenous ferritin colocalizes with RFP-LC3 and Etf-3-GFP in a punctate pattern at 2 dpt. RF/6A cells were cotransfected with a plasmid encoding RFP-LC3 and either Etf-3-GFP (*A*) or GFP (*B*). Ferritin was detected with anti-FTL followed by AF350-conjugated goat anti-rabbit IgG. Each boxed area is enlarged 4× on the right. Ftn is pseudocolored gray in 4× enlarged images. (Scale bars: 10 μm.) (*C*) Colocalization of native ferritin with RFP-LC3-II was analyzed using Pearson's correlation coefficient in transfected RF/6A cells. Results represent the mean ± SD of data for 50 to 60 cells per group from three independent experiments. Asterisk (*): Significantly different by Student's *t* test ($P < 0.05$).

effects of FAC on this process, that is, given that FAC increases cellular ferritin and induces ferritinophagy (47). Ferritin (FTL) level was significantly higher in uninfected or *Ehrlichia*-infected cells that had been treated with FAC (Fig. 9 *A* and *B*), whereas ferritin level was significantly lower in *Ehrlichia*-infected cells than in uninfected cells with or without FAC treatment (Fig. 9 *A* and *B*). *Ehrlichia* infection was determined by WB for the *Ehrlichia* major outer membrane protein P28 (49), as previously described (24), and by qRT-PCR for the *Ehrlichia* 16S rRNA. Treatment with FAC significantly enhanced *Ehrlichia* infection (Fig. 9 *A*, *C*, and *D*) in both assays. These data indicated that *Ehrlichia* induced degradation of ferritin, which promoted the intracellular growth of *Ehrlichia*.

***E. chaffeensis* Infection Depletes the LCI Pool.** As Etf-3–induced ferritinophagy increased the LCI pool (Fig. 8), we examined the amount of the LCI pool in *E. chaffeensis*-infected live cells. In uninfected cells, treatment with FAC significantly expanded the LCI pool (Fig. 10 *A*, *B*, and *E*), whereas, in *E. chaffeensis*-infected cells, the pool remained at the level measured in uninfected cells—regardless of FAC treatment (Fig. 10 *C*–*E*). Furthermore, although Etf-3-GFP overexpression increased the LCI pool in uninfected cells (Figs. 8 and 10*H*) and enhanced *Ehrlichia* infection (Fig. 2) compared with GFP overexpression control, it did not increase the size of the LCI pool in *Ehrlichia*-infected cells (Fig. 10 *F*–*H*). These results indicated that the

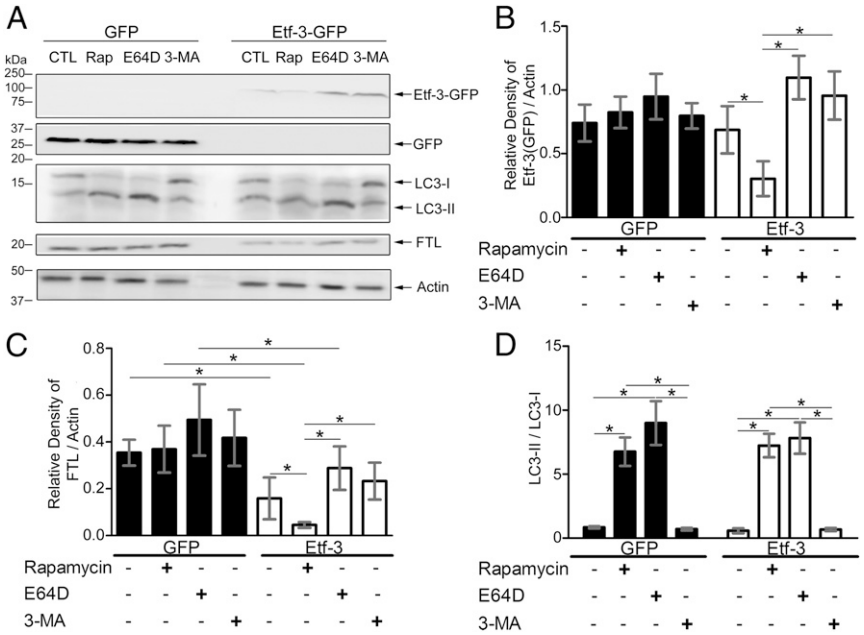

Fig. 6. Etf-3 induces ferritinophagy but not generalized autophagy. (*A*) HEK293 cells were transfected with a plasmid encoding Etf-3-GFP or GFP. Transfected cells were either not treated (CTL) or treated with 3-MA (5 μM), rapamycin (0.1 μM), or E64D (5 μM) 12 h before cell harvest. All treated and nontreated groups were harvested at 2 dpt for WB using antibodies against GFP, actin, FTL, and LC3. (*B*–*D*) Quantification of the relative band densities of Etf-3 (*B*) or FTL (*C*) normalized against human actin, or the band density ratio of LC3-II to LC3-I (*D*). Data indicate the mean ± SD from three independent experiments that had three replicates per sample. Asterisk (*): Significantly different by ANOVA ($P < 0.05$).

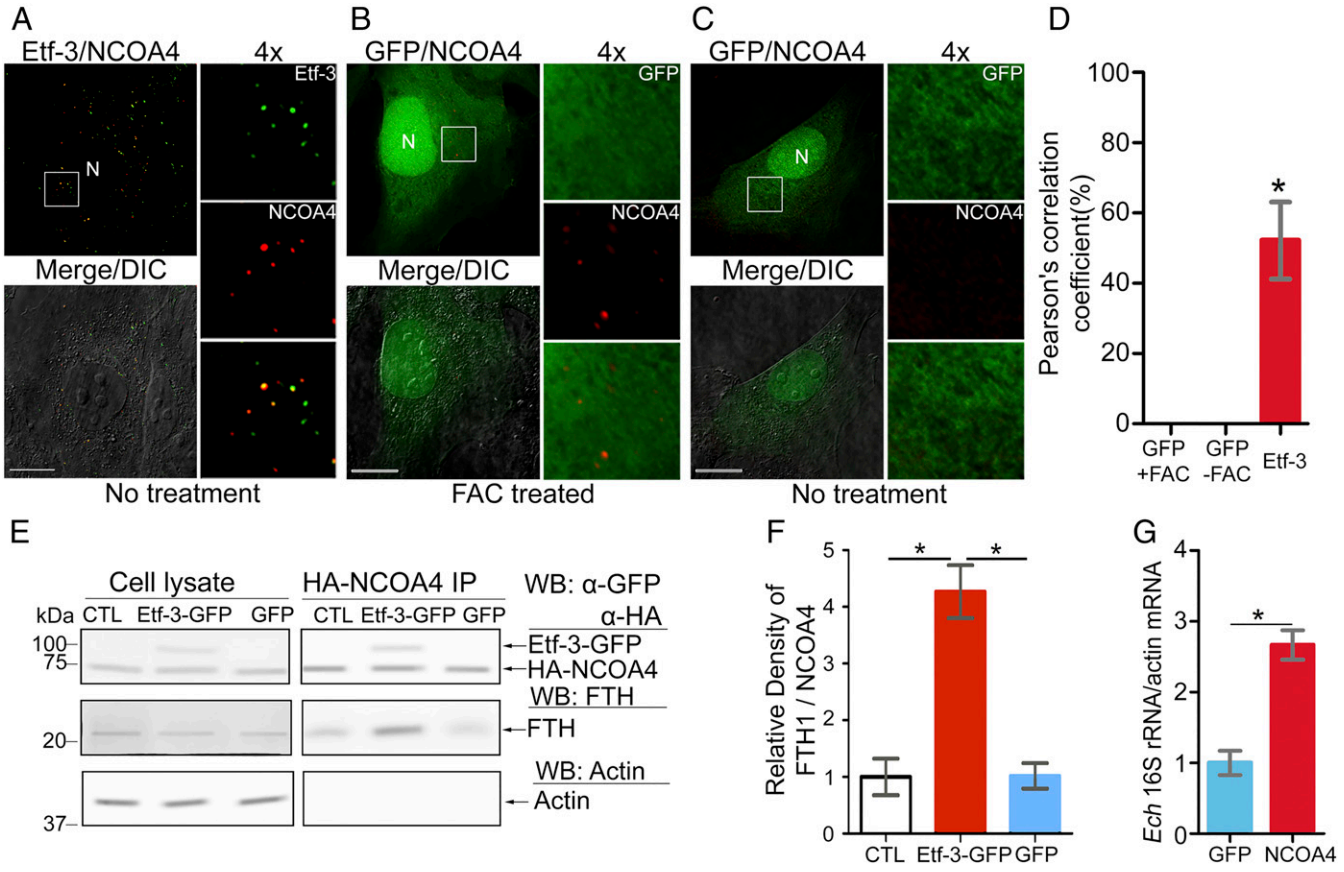

Fig. 7. Etf-3 induces ferritinophagy by facilitating the interaction between ferritin and NCOA4. (*A–C*) Localization of Etf-3 and NCOA4. RF/6A cells were cotransfected with plasmids encoding Etf-3-GFP and HA-NCOA4 (*A*), GFP and HA-NCOA4 with FAC treatment (*B*), or GFP and HA-NCOA4 without FAC treatment (*C*). Each boxed area is enlarged 4× on the right. (Scale bars: 10 μm.) (*D*) Colocalization of HA-NCOA4 with Etf-3-GFP or GFP was analyzed using Pearson's correlation coefficient in transfected RF/6A cells. Results represent the mean ± SD of data for 50 to 60 cells/group from three independent experiments. Asterisk (*): Significantly different by ANOVA ($P < 0.05$). (*E*) HEK293 cells were cotransfected with plasmids encoding HA-NCOA4 and Etf-3-GFP, GFP, or none (CTL). At 2 dpt, cell lysates were immunoprecipitated (IP) with anti-HA–protein A-Sepharose beads, and analyzed by WB with anti-GFP, anti-HA, and anti-FTH1. (*F*) The relative ratio of FTH1 to NCOA4 reflects the mean ± SD from three independent experiments that had three replicates per sample. CTL group was arbitrarily set to 1. Asterisk (*): Significantly different by ANOVA ($P < 0.05$). (*G*) NCOA4 overexpression enhances *E. chaffeensis* infection. HEK293 cells were transfected with a plasmid encoding HA-NCOA4 or GFP control and then infected with *E. chaffeensis* at 1 dpt. *Ehrlichia* were harvested at 2 dpi and subjected to qRT-PCR analysis. The values reflect bacterial 16S rRNA normalized against actin mRNA. Data indicate the mean ± SD from three independent experiments that had three replicates per sample. Asterisk (*): Significantly different by the Student's *t* test ($P < 0.05$).

Fe^{2+} released by ferritinophagy upon treatment with FAC or overexpression of Etf-3 was rapidly consumed by the proliferating *Ehrlichia* and hence removed from the LCI pool.

T4SS Coordinates to Prevent ROS-Induced Damage. As Fe^{3+} is insoluble, it binds to cellular proteins (primarily ferritin). In contrast, although Fe^{2+} is soluble and metabolically available, it generates toxic radicals via the Fenton reaction, which can cause damage to cells; thus, iron levels and redox state are tightly regulated in cells (50). Excessive ferritinophagy leads to ferroptosis owing to the generation of toxic ROS (51), which could presumably kill both *Ehrlichia* and host cells (22), yet we found that Etf-3–induced or FAC-induced ferritinophagy promoted *Ehrlichia* infection (Figs. 2*A*, 7*G*, and 9 *A–D*). Interestingly, the gene encoding *Ehrlichia* Fe-superoxide dismutase (SODB) resides upstream of the T4SS operon (*sodB–virB* operon), which is coregulated by the promoter of *sodB* (52). Also, our previous study revealed that another T4SS effector, Etf-1, up-regulates mitochondrial manganese superoxide dismutase (MnSOD) at the protein level but not the mRNA level, with a consequent reduction in intracellular ROS levels in *Ehrlichia*-infected cells (22). Therefore, we examined whether Etf-3–induced ferritinophagy is coupled to the reduction in cellular ROS via T4SS. To do so, we first ascertained temporal mRNA expression of *Ehrlichia sodB* and T4SS effectors (Etf-3 and Etf-1) and host cell iron homeostasis proteins (ferritin and TfR) in infection-synchronized cultures. In agreement with previous studies (22, 52, 53), SODB, Etf-1, and Etf-3 mRNAs were synchronously up-regulated at the beginning of the exponential *Ehrlichia* growth stage and decreased during the short stationary growth stage prior to host cell lysis (*SI Appendix*, Fig. S7). Thus, during exponential growth of *Ehrlichia*, ROS are likely maintained at low levels via T4SS-linked pathway. In contrast, FTL and FTH1 mRNAs increased gradually and peaked during the stationary *Ehrlichia* growth stage, corroborating the observation of diminished cellular ferritin at the posttranscriptional level by ferritinophagy. TfR mRNA was up-regulated during the lag phase, peaked at the end of lag phase, and then decreased, as reported (13), supporting the assertion that ferritin is the primary source of iron for exponential growth of *Ehrlichia*.

Next, we examined cellular ROS levels and *Ehrlichia* SODB and host mitochondrial MnSOD levels in *Ehrlichia*-infected cells with or without FAC-induced ferritinophagy. We quantified cellular ROS levels in *Ehrlichia*-infected cells with or without FAC treatment using H_2DCFDA (2′,7′-dichlorodihydrofluorescein

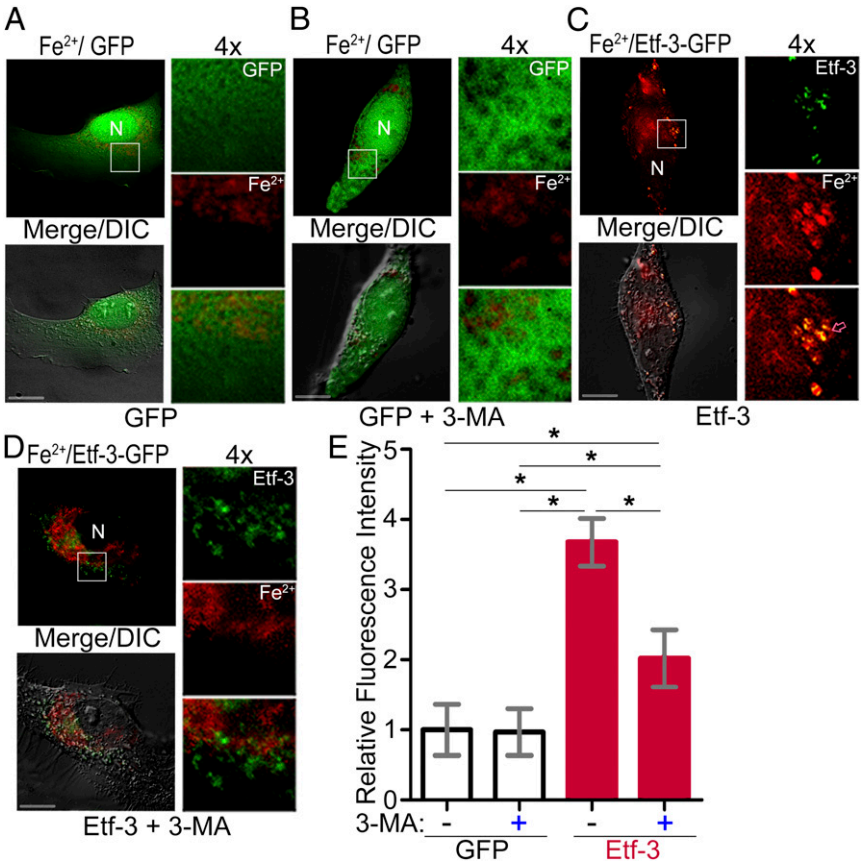

Fig. 8. Etf-3 increases the LCI pool via ferritinophagy. (*A–D*) RF/6A cells were transfected with a plasmid encoding GFP control (*A* and *B*) or Etf-3-GFP (*C* and *D*), and then cells were either not treated (*A* and *C*) or treated with 3-MA 12 h before live cell imaging (*B* and *D*). Intracellular Fe^{2+} was detected with BioTracker 575 Red Fe^{2+} dye. Live cells were observed under a DeltaVision microscope at 37 °C. The pink open arrow indicates the colocalization of Etf-3 with Fe^{2+} (*C*). Each boxed area is enlarged 4× on the right. (*E*) The red fluorescence intensity was analyzed with ImageJ software. GFP control was arbitrarily set as 1. Results reflect average values for 50 to 60 cells per group ± SD from three independent experiments. Asterisk (*): Significantly different by ANOVA ($P < 0.05$).

diacetate), which permeates the host cell plasma membrane and becomes trapped inside cells after hydrolysis by cellular esterases to yield membrane-impermeable H_2DCF. H_2DCF can be oxidized by ROS to yield DCF, which is detectable by fluorescence spectrophotometry (54). In uninfected cells, FAC treatment strongly induced ROS at 24 h posttreatment (Fig. 11*A*), but ROS levels were significantly reduced in *Ehrlichia*-infected cells even with FAC treatment (Fig. 11*A*). Further, both SODB mRNA and MnSOD were up-regulated in infected cells that had been treated with FAC (Fig. 11 *B–D*). Thus, *Ehrlichia* infection also couples FAC-induced ferritinophagy with the reduction in cellular ROS via T4SS-linked signaling to accelerate bacterial proliferation.

Etf-1 Synergizes with Etf-3 to Enhance Ferritinophagy and Minimize ROS Production. Etf-1 is an abundant *Ehrlichia* T4SS effector that induces RAB5-regulated autophagy (in addition to up-regulating MnSOD) (9, 55). Because rapamycin augmented Etf-3–induced ferritinophagy (Fig. 6 *A* and *C*), we examined whether Etf-1 could enhance ferritinophagy activated by Etf-3. Indeed, cotransfection of cells with Etf-1 and Etf-3 enhanced Etf-3–activated ferritinophagy (as represented by endogenous FTL degradation) (*SI Appendix*, Fig. S8 *A–C*), indicating that Etf-1 synergizes with Etf-3 to promote ferritinophagy. However, Etf-1 alone did not significantly induce ferritinophagy (*SI Appendix*, Fig. S8 *A* and *B*). Although Etf-3–induced ferritinophagy did not lead to any significant global change in the LC3-II:LC3-I ratio (Fig. 6 *A* and *D*), cotransfection with Etf-1 and Etf-3 increased the ratio as high as upon transfection of cells with Etf-1 alone (9) (*SI Appendix*, Fig. S8 *A* and *C*). Slightly reduced LC3-II:LC3-I ratio in Etf-1 and Etf-3 cotransfected cells compared with Etf-1 alone transfected cells was likely due to slightly reduced Etf-1 expression in cotransfected cells (*SI Appendix*, Fig. S8 *A* and *C*). A portion of secreted Etf-1 enters host cell mitochondria and up-regulates mitochondrial matrix MnSOD by stabilizing it at the protein level, thereby reducing cellular ROS levels (22). Etf-1 alone—with or without FAC treatment—led to a significant decrease in intracellular ROS levels compared with the negative-control HA-plasmid $RAB5^{S/N}$ (*SI Appendix*, Fig. S8*D*). In contrast, Etf-3 alone—with or without FAC—led to a significant increase in intracellular ROS levels compared with HA-plasmid $RAB5^{S/N}$ group (*SI Appendix*, Fig. S8*D*). However, coexpression of Etf-3 and Etf-1 led to a significant reduction in Etf-3–induced intracellular ROS levels with or without FAC treatment (*SI Appendix*, Fig. S8*D*).

Discussion

Iron is a key determinant of infection by pathogenic microbes, which have evolved various mechanisms to competitively acquire iron from host cells (56). For intracellular pathogens of eukaryotic cells, acquiring iron is a balancing act, as the acquisition must not damage or kill the host cells until pathogen proliferation reaches a critical level. Well-known strategies for this are as follows: 1) siderophores, which are high-affinity iron-chelating compounds that capture and transport iron across cell membranes; siderophores are utilized by many facultative intracellular bacteria, for example, *Mycobacterium*, *Brucella*, *Legionella*, *Salmonella*, *Yersinia*, *Burkholderia*, *Listeria*, and *Shigella* (56–61); 2) hemin binding/uptake (*Legionella*, *Yersinia*,

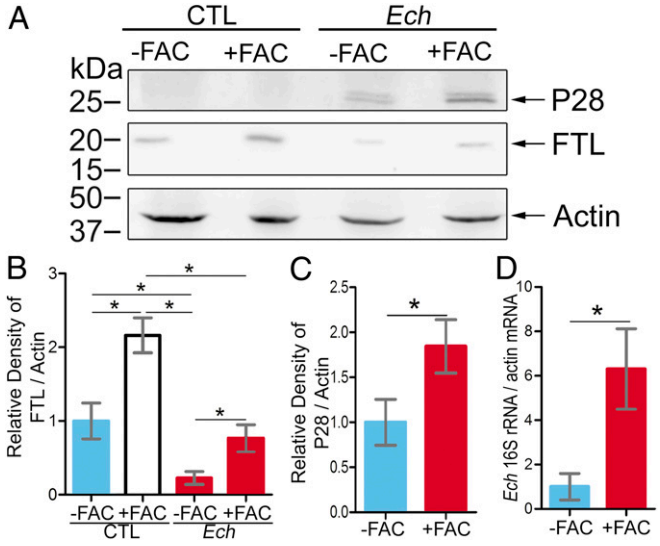

Fig. 9. *Ehrlichia* infection causes degradation of ferritin, and increased cellular ferritin significantly enhances *Ehrlichia* infection. (*A*) WB using anti-P28 (*Ech* major protein), anti-FTL, and anti-actin. Uninfected (CTL) or *E. chaffeensis* (*Ech*)-infected THP-1 cells were at 1 d pi, were either not treated (–) or treated (+) with 40 μM FAC and harvested 1.5 d later. (*B* and *C*) Relative band density ratios of FTL (*B*) or P28 (*C*) relative to actin. CTL-FAC (*B*) or *Ech*-FAC (*C*) was arbitrarily set to 1. (*D*) The qRT-PCR of *E. chaffeensis* 16S rRNA normalized against human actin mRNA. The nontreated group was arbitrarily set to 1. In *B–D*, data indicate the mean ± SD from three independent experiments. Asterisk (*): Significantly different by ANOVA or Student's *t* test ($P < 0.05$).

Burkholderia) (62, 63); 3) iron released from Tf in endosomes is taken up (*Chlamydia*) (64, 65); and 4) iron released from host iron-binding proteins in the acidic degradative *Coxiella*-containing compartment (*Coxiella*) (66). The present study reveals an unprecedented mechanism of iron acquisition, namely, ferritinophagy, which evolved in *Ehrlichia*. Central to this mechanism is the *Ehrlichia* protein Etf-3, which is the first bacterial effector that has been demonstrated to modulate ferritin by ferritinophagy. The diminution of ferritin in *Ehrlichia*-infected cells is striking compared to Etf-3-GFP–transfected cells. This is most likely because 1) the Etf-3-GFP transfection is transient, whereas, in *Ehrlichia*-infected cells, Etf-3 is increasingly produced/secreted during bacterial replication, and 2) Etf-1–induced autophagy synergizes with Etf-3–induced ferritinophagy in infected host cells.

Iron metabolism is tightly regulated at the organismal level by hormones and cytokines; at the cellular level, intracellular iron distribution is regulated transcriptionally and posttranscriptionally via iron sensors, iron-binding molecules, and iron transporters (37). Furthermore, host cells can sequester iron from invading pathogens, which constitutes a protective mechanism termed "nutritional immunity" (67). Nonetheless, *Ehrlichia* stabilizes TfR mRNA by activating iron-responsive protein 1 in human macrophages (13). In turn, interferon-γ–activated macrophages can inhibit *Ehrlichia* infection by down-regulating TfR mRNA (12). However, this initial battle between *Ehrlichia* and host cells for iron ends during exponential growth of *Ehrlichia*, without obvious damage on host cells until they rupture owing to overwhelming infection (13). The present study reveals that T4SS, especially Etf-3–induced ferritinophagy, is the key mechanism by which *Ehrlichia* overwhelms the host cell iron homeostasis and nutritional immunity defenses.

Soluble iron Fe^{2+} is initially recruited to ferritin for storage, and its conversion to Fe^{3+} helps prevent the generation of ROS (68, 69). Ferritin degradation occurs primarily in lysosomes (70), with a possible minor contribution from proteasome-mediated degradation (71). To release iron from ferritin, the ironbound form is sequestered within an autophagosome (72). This process is called ferritinophagy, a selective form of autophagy that functions in intracellular iron processing (47). NCOA4 is a cargo receptor that recruits ferritin to the autophagosome (47). The present study reveals that *Ehrlichia* highjacks cellular iron homeostasis, that is, the NCOA4-mediated ferritinophagy mechanism for *Ehrlichia* proliferation. Details of the molecular mechanism, by which Etf-3 binding to human holoferritin recruits NCOA4 and LC3, remain to be elucidated.

Fusion of ferritin-containing autophagosomes with lysosomes leads to ferritin breakdown and iron release. Furthermore, iron can be acidified in the lysosome, converting it from the Fe^{3+}

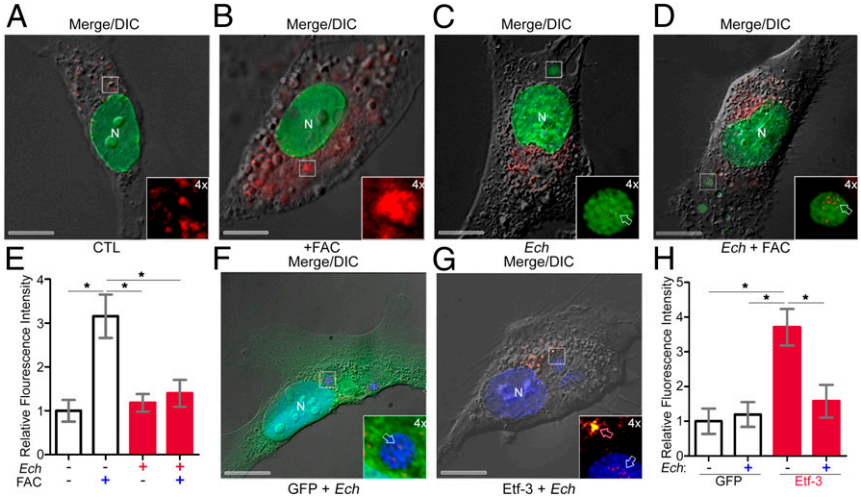

Fig. 10. *E. chaffeensis* infection depletes the LCI pool. Uninfected (*A* and *B*) or *E. chaffeensis* (*Ech*)-infected (*C* and *D*) RF/6A cells at 1 d pi were either not treated (*A* and *C*) or treated with 40 μM FAC (*B* and *D*) and harvested 1.5 d later. (*F–H*) RF/6A cells were transfected with a plasmid encoding GFP (*F*) or Etf-3-GFP (*G*) and infected with *E. chaffeensis* at 1 dpt and then harvested at 1.5 dpi. Intracellular Fe^{2+} was detected with BioTracker 575 Red Fe^{2+} dye (red). Live cells were observed at 37 °C. DNA (nucleus and *E. chaffeensis*) was stained with Hoechst 33342 (pseudocolored green in *A–D*). White open arrows indicate Fe^{2+} inside *Ehrlichia* inclusions (*C*, *D*, and *F*), and pink open arrow indicates colocalization of Etf-3-GFP and Fe^{2+} (*G*). Each boxed area is enlarged 4× in *Inset*. (Scale bars: 10 μm.) (*E* and *H*) The red fluorescence intensity was analyzed with ImageJ software. Untreated or GFP-transfected uninfected control was arbitrarily set as 1. Results reflect average values for 50 to 60 cells per group ± SD from three independent experiments. Asterisk (*): Significantly different by ANOVA ($P < 0.05$).

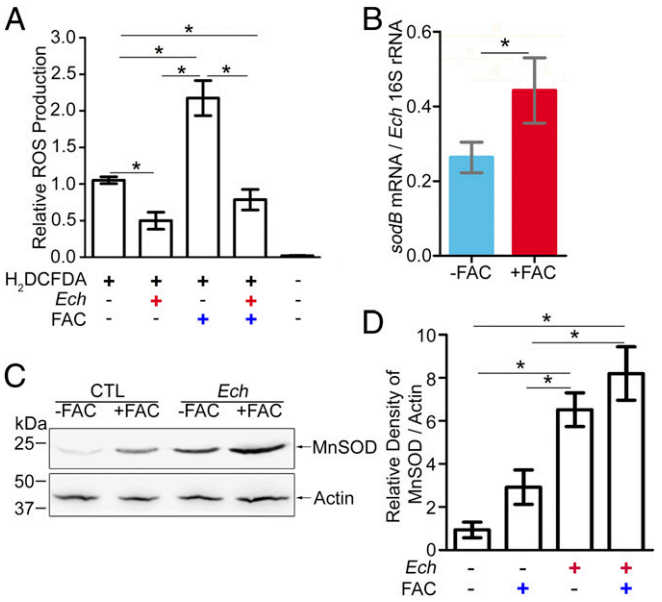

Fig. 11. Excess LCI pool can increase intracellular ROS production, while this process can be attenuated by *E. chaffeensis* infection. (*A*) *E. chaffeensis* infection reduces ROS levels with or without FAC treatment. HEK293 cells were infected with *E. chaffeensis* for 1 d and treated with 40 μM FAC for 1 d. ROS production was analyzed with the fluorescent indicator H_2DCFDA. (*B*) The qRT-PCR of SODB mRNA expression by *E. chaffeensis* with or without FAC treatment normalized to 16S rRNA. (*C* and *D*) WB of *E. chaffeensis*-infected HEK293 cells with or without FAC treatment using anti-MnSOD and anti-actin. (*D*) Relative band density ratios of MnSOD to actin. The value for the noninfected (–) cells without FAC treatment was arbitrarily set to 1. In *A*, *B*, and *D*, data are presented as the mean ± SD from three independent experiments that had three replicates per sample. Asterisk (*): Significantly different by the Student's *t* test or ANOVA ($P < 0.05$).

inactive state to the Fe^{2+} active state (73, 74). Iron can be detected in autolysosomes via transmission electron microscopy (74). The present study employed a method to localize and quantify intracellular Fe^{2+} using BioTracker 575 Red Fe^{2+} dye labeling in live cells. This approach indeed demonstrated a significant increase of LCI Fe^{2+} in Etf-3–transfected cells. Importantly, Fe^{2+} levels were lower in *Ehrlichia*-infected cells, suggesting rapid assimilation of Fe^{2+} and conversion to *Ehrlichia* protein-bound Fe^{3+} in proliferating *Ehrlichia* as shown schematically in *SI Appendix*, Fig. S9.

Transcription of the *etf-3* gene is required for *Ehrlichia* infection, and ectopic expression of Etf-3 and NCOA4, as well as FAC treatment, enhanced *Ehrlichia* infection, indicating that Etf-3–induced ferritinophagy is not an incidental phenomenon but is indeed required for infection. Consequently, Etf-3 is a potential therapeutic target for ehrlichiosis. In this respect, the present study reveals the reason why 3-MA, which blocks autophagosome nucleation, is one of most effective compounds (other than doxycycline) to block *Ehrlichia* infection in vitro (9); it blocks *Ehrlichia* acquisition of amino acids via Etf-1–induced autophagy (9) and acquisition of iron via Etf-3–induced ferritinophagy. Thus, *Ehrlichia* inclusions appear to be highly efficient recycling centers inside the host cell, and a compound that could block this recycling process, that is, which is induced specifically via T4SS, would be expected to be highly effective for inhibiting *Ehrlichia* proliferation.

Under aerobic conditions, high concentrations of intracellular Fe^{2+} are toxic because they lead to the production of highly toxic hydroxyl radicals by the Fenton reaction. The hydroxyl radicals then react with a toxic reactive nitrogen species, for example, nitric oxide, to generate additional ROS. ROS and reactive nitrogen species can covalently modify proteins, RNA, and DNA to impair their functions, and thus ROS is a powerful antimicrobial arsenal, but uncontrolled ROS and reactive nitrogen species cause cell death (51). The results of the present study reveal that, to minimize damage to both bacteria and host cells, *Ehrlichia* counteract the Etf-3-induced increase in LCI by two mechanisms: 1) rapid assimilation of liberated Fe^{2+} for bacterial growth, so LCI levels are kept low, and 2) increased production of both bacterial and host SODs in concert with Etf-3 secretion. This synchronization is possible as *Ehrlichia* and host SOD and Etf-3 are coregulated in T4SS, indicating that a novel means of T4SS-linked regulation of cellular and bacterial factors evolved in obligatory intracellular bacteria. This underscores the idea that the obligatory intracellular bacteria cannot afford to kill host cells.

The present study supports the concept of synergism between T4SS effectors. Although only three effectors have been studied in *E. chaffeensis*, all of them synergize to promote *Ehrlichia* infection. Etf-2 retains RAB5 in the GTP-bound/active state to prevent fusion of *Ehrlichia* inclusions with lysosomes (24). Simultaneously, RAB5-GTP binds the RAB5 effector VPS34 to enhance RAB5-regulated autophagy induced by Etf-1, which provides catabolites for *Ehrlichia* growth (9), and Etf-1 enhances Etf-3–induced ferritinophagy (this study; *SI Appendix*, Fig. S8) and, by translocating into mitochondria Etf-1, increases the cellular level of host mitochondrial MnSOD (22) to detoxify cellular ROS generated via Etf-3–induced ferritinophagy (this study; *SI Appendix*, Fig. S8) and via aerobic respiration by host cell mitochondria (22). Based on our global transcriptome analysis using RNA sequencing of exponentially growing *E. chaffeensis* Arkansas in DH82 canine macrophages (GEO accession #GSE56339, https://www.ncbi.nlm.nih.gov/geo/query/acc.cgi?acc=GSE56339), expression levels of Etf mRNAs follows the trend Etf-1 > Etf-2 > Etf-3. Our global proteomics analysis of exponentially growing *E. chaffeensis* Arkansas in HL-60 human promyelocytic leukemia cells showed a similar trend (26), suggesting that the Etf-3 level is kept low to prevent ROS-induced cellular damage. As our study reveals that both ferritin and Etf-3 are degraded during Etf-3–induced ferritinophagy, this itself also limits the cellular level of Etf-3 in *Ehrlichia*-infected cells. *Ehrlichia* spp. replicate in ticks, which feed on blood, an iron-rich meal, suggesting that Etf-3 and other T4SS effectors have important roles in tick stage and, thus, transmission of *Ehrlichia* as well.

In conclusion, our findings indicate that an intracellular bacterial molecule facilitates the hijacking of the host cell control of ferritinophagy to establish an infection, which can be exploited for antimicrobial therapy, more broadly for treating iron storage disorders, and for understanding the molecular mechanisms of ferritinophagy.

Materials and Methods

Additional experimental details are provided as *SI Appendix, Supplemental Materials and Methods*.

Bacteria, Cell Culture, and Antibodies. *E. chaffeensis* Arkansas strain (75) was cultured in THP-1 cells (American Type Culture Collection) (12). The detailed culture method and list of antibodies used are provided in *SI Appendix*.

Cloning. Genes encoding Etf-3 and FTH1 were PCR amplified from *E. chaffeensis* genomic DNA and cDNA from THP-1 cells, respectively, and subsequently cloned into pET33b(+) (Novagen) to create plasmids expressing 6×His-tagged Etf-3 and FTH1. For expression in mammalian cells, full-length Etf-3 was codon optimized, custom synthesized (GenScript; *SI Appendix*, Table S1), and recloned into pEGFP-N1 (Takara) to create a plasmid encoding Etf-3-GFP. The HA-Etf-3 mammalian expression vector was constructed from the Etf-3-GFP plasmid, and the HA-NCOA4 mammalian expression vector was constructed from cDNA from THP-1 cells using two-step

PCR with overlapping primers (*SI Appendix*, Table S1) and subsequently cloned into pEGFP-N1 by replacing the GFP tag.

Transformation of *E. chaffeensis* with FLAG-Etf-3 or FLAG-Etf-3ΔC Himar Plasmid. The pCis-FLAG-Etf-3-SS-Himar A7 or pCis-FLAG-Etf-3ΔC-SS-Himar A7 plasmid encoding FLAG-tagged Etf-3 or Etf-3ΔC (residues 1 to 588; Etf-3 with C-terminal T4SS signal deletion), respectively, and the spectinomycin/streptomycin antibiotic resistance gene (*aad*) were created from the pCis-FLAG-Etf-2-SS-Himar A7 plasmid (24, 30, 76). The detailed method is described in *SI Appendix*.

Production of Llama Antisera against Etf-3 and Native Etf-3 Expression Analysis in *E. chaffeensis*–Infected RF/6A Cells. The detailed method is described in *SI Appendix*.

PNA Synthesis, Biotin Labeling, RNA–PNA Hybridization, PNA Transfection of Host Cell–free *E. chaffeensis*, and Knockdown and Complementation Analysis. The detailed method is described in *SI Appendix*.

Effect of Etf-3-GFP and NCOA4 Overexpression on *E. chaffeensis* Infection. The detailed method is described in *SI Appendix*.

Yeast Two-Hybrid Assay. Codon-optimized, full-length Etf-3 was cloned into vector pGBKT7 (Takara) and transformed into *Saccharomyces cerevisiae* Y187 using the Quick & Easy yeast transformation kit (Takara). Human Leukocyte Matchmaker cDNA Library (Takara) was amplified and transformed into *S. cerevisiae* AH109. The detailed method is described in *SI Appendix*.

Far-WB, Coimmunoprecipitation, and WB. The detailed method is described in *SI Appendix*.

Open SPR. Binding experiments were carried out with an OpenSPR system (Nicoya Lifesciences). The rEtf-3 was labeled with biotin via EZ-Link NHS-Biotin Reagents (ThermoFisher Scientific) and immobilized on a streptavidin sensor chip via noncovalent coupling at a final concentration of 10 μg/mL. Measurements were then made as described in the user manual (Nicoya Lifesciences). The detailed method is described in *SI Appendix*.

Ferritinophagy Analysis. DH82 or HEK293 cells were transfected with Etf-3-GFP, Etf-1-GFP, or GFP plasmid by electroporation. Twelve hours prior to harvesting, transfected HEK293 cells were treated with rapamycin (Sigma-Aldrich), E64D (Sigma-Aldrich), or 3-MA (Sigma-Aldrich). Cell lysates were prepared as described above and subjected to WB with anti-actin and anti-FTL. The detailed method is described in *SI Appendix*.

Cellular Localization Analysis. DH82 cells were electroporated with Etf-3-GFP or GFP plasmid, and either left untreated or treated with 40 μM FAC (ThermoFisher Scientific) for 24 h prior to harvesting at 2 d posttransfection (dpt). Cells were cytocentrifuged on slides and fixed with 4% paraformaldehyde and incubated with rabbit anti-FTL in PGS (phosphate-buffered saline supplemented with 0.5% bovine serum albumin [Sigma], 0.1% gelatin [Sigma], and 0.1% saponin [Sigma]) followed by AF555-conjugated goat anti-rabbit IgG in PGS. RF/6A cells were cotransfected with plasmids encoding Etf-3-GFP/GFP and RFP-LC3 or RFP-FTL using Lipofectamine 3000 (Invitrogen). For colocalization analysis of RFP-LC3 and endogenous ferritin with/without Etf-3-GFP, RF/6A cells were cultured on coverslips in wells of a 24-well plate and cotransfected with plasmids encoding RFP-LC3 and Etf-3-GFP or GFP. Cells were incubated with rabbit anti-FTL followed by AF350-conjugated goat anti-rabbit IgG in PGS. For colocalization analysis of Etf-3-GFP and HA-NCOA4, RF/6A cells were cotransfected with plasmids encoding HA-NCOA4 and Etf-3-GFP or GFP. Cells were labeled with mouse anti-HA in PGS followed by AF555-conjugated goat anti-mouse IgG in PGS. Fluorescence images with overlay differential interference contrast (DIC) images were acquired and analyzed with a DeltaVision PersonalDV deconvolution microscope system (GE Healthcare Life Sciences). Colocalization analysis was performed with Coloc 2 in the NIH Image J software package to calculate the Pearson correlation coefficient. The detailed method is described in *SI Appendix*.

Estimating LCI in Live Cells. Etf-3-GFP–transfected or GFP-transfected RF/6A cells were seeded and grown in a 35-mm chambered glass-bottomed culture dish (WillCo Wells) and infected with *E. chaffeensis*, treated with 40 μM FAC 1 d prior to testing, or treated with 2 mM 3-MA 12 h prior to testing. Cells were incubated with 5 μM BioTracker 575 Red Fe^{2+} dye (Sigma-Aldrich) at 37 °C for 1 h. Nuclei and *E. chaffeensis* were labeled with Hoechst 33342 (Sigma-Aldrich) at 37 °C for 15 min. Then, cells were washed with Hanks' balanced salt solution (Sigma-Aldrich). Live cells were observed under a DeltaVision microscope at 37 °C. The red fluorescence intensity was analyzed with ImageJ software. The detailed method is described in *SI Appendix*.

Synchronous Culture of *E. chaffeensis*. Human monocyte cell line was synchronously infected with *E. chaffeensis* as described (22). The detailed method is described in *SI Appendix*.

E. chaffeensis growth (16S rRNA) and expression of *etf-3*, *etf-1*, *sodb*, *ftl*, *fth*, *tfr*, and *actin* (*ActB*) were determined by qRT-PCR analysis using specific primers (*SI Appendix*, Table S2).

Analysis of Intracellular Levels of ROS, and MnSOD, and SODB mRNA. HEK293 cells were seeded in a 96-well plate (Tecan). Intracellular ROS were determined at 2 d postinfection (dpi) by using the fluorescent dye H_2DCFDA (Invitrogen) as described (22). The fluorescence intensity of DCF, corresponding to the ROS level, was measured with a Tecan Microplate Reader (Infinite 200 PRO, Tecan) at excitation and emission wavelengths of 492 nm and 520 nm, respectively. The amount of MnSOD was estimated by WB, and SODB mRNAs were determined by qRT-PCR. The detailed method is described in *SI Appendix*.

Data Availability. All study data are included in the article and *SI Appendix*.

ACKNOWLEDGMENTS. We thank Dr. Kavita Lole at Indian Council of Medical Research, National Institute of Virology, Pune, India, for providing plasmid encoding RFP-FTL. This study was funded by Grant R01AI151065 to Y.R. from the NIH.

1. C. I. Paules, H. D. Marston, M. E. Bloom, A. S. Fauci, Tickborne diseases–Confronting a growing threat. *N. Engl. J. Med.* **379**, 701–703 (2018).
2. H. M. Biggs *et al.*, Diagnosis and management of tickborne rickettsial diseases: Rocky Mountain spotted fever and other spotted fever group rickettsioses, ehrlichioses, and anaplasmosis–United States. *MMWR Recomm. Rep.* **65**, 1–44 (2016).
3. N. S. Havens, B. R. Kinnear, S. Mató, Fatal ehrlichial myocarditis in a healthy adolescent: A case report and review of the literature. *Clin. Infect. Dis.* **54**, e113–e114 (2012).
4. C. D. Paddock, J. E. Childs, *Ehrlichia chaffeensis*: A prototypical emerging pathogen. *Clin. Microbiol. Rev.* **16**, 37–64 (2003).
5. S. P. Whitt, E. D. Everett, W. Roland, S. Dolan, *Ehrlichia chaffeensis*—Associated cardiomyopathy in a patient with AIDS. *Clin. Infect. Dis.* **28**, 140 (1999).
6. R. T. Jackson, J. W. Jackson, Ehrlichiosis with systemic sepsis syndrome. *Tenn. Med.* **90**, 185–186 (1997).
7. R. E. Barnewall, Y. Rikihisa, E. H. Lee, *Ehrlichia chaffeensis* inclusions are early endosomes which selectively accumulate transferrin receptor. *Infect. Immun.* **65**, 1455–1461 (1997).
8. J. Mott, R. E. Barnewall, Y. Rikihisa, Human granulocytic ehrlichiosis agent and *Ehrlichia chaffeensis* reside in different cytoplasmic compartments in HL-60 cells. *Infect. Immun.* **67**, 1368–1378 (1999).
9. M. Lin *et al.*, Ehrlichia secretes Etf-1 to induce autophagy and capture nutrients for its growth through RAB5 and class III phosphatidylinositol 3-kinase. *Autophagy* **12**, 2145–2166 (2016).
10. J. Kaplan, D. M. Ward, The essential nature of iron usage and regulation. *Curr. Biol.* **23**, 2325 (2013).
11. J. C. Dunning Hotopp *et al.*, Comparative genomics of emerging human ehrlichiosis agents. *PLoS Genet.* **2**, e21 (2006). Correction in: *PLoS Genet.* **2**, e213 (2006).
12. R. E. Barnewall, Y. Rikihisa, Abrogation of gamma interferon-induced inhibition of *Ehrlichia chaffeensis* infection in human monocytes with iron-transferrin. *Infect. Immun.* **62**, 4804–4810 (1994).
13. R. E. Barnewall, N. Ohashi, Y. Rikihisa, *Ehrlichia chaffeensis* and *E. sennetsu*, but not the human granulocytic ehrlichiosis agent, colocalize with transferrin receptor and up-regulate transferrin receptor mRNA by activating iron-responsive protein 1. *Infect. Immun.* **67**, 2258–2265 (1999).
14. E. Grohmann, P. J. Christie, G. Waksman, S. Backert, Type IV secretion in gram-negative and gram-positive bacteria. *Mol. Microbiol.* **107**, 455–471 (2018).
15. C. E. Alvarez-Martinez, P. J. Christie, Biological diversity of prokaryotic type IV secretion systems. *Microbiol. Mol. Biol. Rev.* **73**, 775–808 (2009).

MICROBIOLOGY

16. J. J. Gillespie *et al*., The *Rickettsia* type IV secretion system: Unrealized complexity mired by gene family expansion. *Pathog. Dis.* **74**, ftw058 (2016).
17. A. Hubber, C. R. Roy, Modulation of host cell function by *Legionella pneumophila* type IV effectors. *Annu. Rev. Cell Dev. Biol.* **26**, 261–283 (2010).
18. Y. Rikihisa, Role and function of the type IV secretion system in anaplasma and Ehrlichia species. *Curr. Top. Microbiol. Immunol.* **413**, 297–321 (2017).
19. O. H. Voss *et al*., Risk1, a phosphatidylinositol 3-kinase effector, promotes *Rickettsia typhi* intracellular survival. *mBio* **11**, e00820-20 (2020).
20. S. S. Lehman *et al*., The rickettsial ankyrin repeat protein 2 is a type IV secreted effector that associates with the endoplasmic reticulum. *mBio* **9**, e00975-18 (2018).
21. K. E. Rennoll-Bankert *et al*., Which way in? The RalF Arf-GEF orchestrates *Rickettsia* host cell invasion. *PLoS Pathog.* **11**, e1005115 (2015).
22. H. Liu, W. Bao, M. Lin, H. Niu, Y. Rikihisa, *Ehrlichia* type IV secretion effector ECH0825 is translocated to mitochondria and curbs ROS and apoptosis by upregulating host MnSOD. *Cell. Microbiol.* **14**, 1037–1050 (2012).
23. P. Sharma, O. Teymournejad, Y. Rikihisa, Peptide nucleic acid knockdown and intra-host cell complementation of *Ehrlichia* type IV secretion system effector. *Front. Cell. Infect. Microbiol.* **7**, 228 (2017).
24. Q. Yan *et al*., *Ehrlichia* type IV secretion system effector Etf-2 binds to active RAB5 and delays endosome maturation. *Proc. Natl. Acad. Sci. U.S.A.* **115**, E8977–E8986 (2018).
25. I. K. Jordan, I. B. Rogozin, Y. I. Wolf, E. V. Koonin, Essential genes are more evolutionarily conserved than are nonessential genes in bacteria. *Genome Res.* **12**, 962–968 (2002).
26. M. Lin, T. Kikuchi, H. M. Brewer, A. D. Norbeck, Y. Rikihisa, Global proteomic analysis of two tick-borne emerging zoonotic agents: *Anaplasma phagocytophilum* and *Ehrlichia chaffeensis*. *Front. Microbiol.* **2**, 24 (2011).
27. J. A. Kuriakose, S. Miyashiro, T. Luo, B. Zhu, J. W. McBride, *Ehrlichia chaffeensis* transcriptome in mammalian and arthropod hosts reveals differential gene expression and post transcriptional regulation. *PLoS One* **6**, e24136 (2011).
28. E. E. McClure *et al*., Engineering of obligate intracellular bacteria: Progress, challenges and paradigms. *Nat. Rev. Microbiol.* **15**, 544–558 (2017).
29. A. C. Vergunst *et al*., Positive charge is an important feature of the C-terminal transport signal of the VirB/D4-translocated proteins of Agrobacterium. *Proc. Natl. Acad. Sci. U.S.A.* **102**, 832–837 (2005).
30. C. Cheng *et al*., Targeted and random mutagenesis of *Ehrlichia chaffeensis* for the identification of genes required for in vivo infection. *PLoS Pathog.* **9**, e1003171 (2013).
31. M. Egholm *et al*., PNA hybridizes to complementary oligonucleotides obeying the Watson–Crick hydrogen-bonding rules. *Nature* **365**, 566–568 (1993).
32. P. E. Nielsen, M. Egholm, O. Buchardt, Sequence-specific transcription arrest by peptide nucleic acid bound to the DNA template strand. *Gene* **149**, 139–145 (1994).
33. C. Gambacorti-Passerini *et al*., In vitro transcription and translation inhibition by anti-promyelocytic leukemia (PML)/retinoic acid receptor alpha and anti-PML peptide nucleic acid. *Blood* **88**, 1411–1417 (1996).
34. L. Good, P. E. Nielsen, Antisense inhibition of gene expression in bacteria by PNA targeted to mRNA. *Nat. Biotechnol.* **16**, 355–358 (1998).
35. P. E. Nielsen, M. Egholm, An introduction to peptide nucleic acid. *Curr. Issues Mol. Biol.* **1**, 89–104 (1999).
36. P. Arosio, R. Ingrassia, P. Cavadini, Ferritins: A family of molecules for iron storage, antioxidation and more. *Biochim. Biophys. Acta* **1790**, 589–599 (2009).
37. A. R. Bogdan, M. Miyazawa, K. Hashimoto, Y. Tsuji, Regulators of iron homeostasis: New players in metabolism, cell death, and disease. *Trends Biochem. Sci.* **41**, 274–286 (2016).
38. C. C. Philpott, The flux of iron through ferritin in erythrocyte development. *Curr. Opin. Hematol.* **25**, 183–188 (2018).
39. T. Z. Kidane, E. Sauble, M. C. Linder, Release of iron from ferritin requires lysosomal activity. *Am. J. Physiol. Cell Physiol.* **291**, C445–C455 (2006).
40. Y. Kabeya *et al*., LC3, a mammalian homologue of yeast Apg8p, is localized in autophagosome membranes after processing. *EMBO J.* **19**, 5720–5728 (2000).
41. Y. Kabeya *et al*., LC3, GABARAP and GATE16 localize to autophagosomal membrane depending on form-II formation. *J. Cell Sci.* **117**, 2805–2812 (2004).
42. C. H. Jung, S. H. Ro, J. Cao, N. M. Otto, D. H. Kim, mTOR regulation of autophagy. *FEBS Lett.* **584**, 1287–1295 (2010).
43. P. O. Seglen, P. B. Gordon, 3-Methyladenine: Specific inhibitor of autophagic/lysosomal protein degradation in isolated rat hepatocytes. *Proc. Natl. Acad. Sci. U.S.A.* **79**, 1889–1892 (1982).
44. E. J. Murray, M. S. Grisanti, G. V. Bentley, S. S. Murray, E64d, a membrane-permeable cysteine protease inhibitor, attenuates the effects of parathyroid hormone on osteoblasts in vitro. *Metabolism* **46**, 1090–1094 (1997).
45. I. Tanida, T. Ueno, E. Kominami, LC3 and autophagy. *Methods Mol. Biol.* **445**, 77–88 (2008).
46. N. Mizushima, T. Yoshimori, How to interpret LC3 immunoblotting. *Autophagy* **3**, 542–545 (2007).
47. J. D. Mancias, X. Wang, S. P. Gygi, J. W. Harper, A. C. Kimmelman, Quantitative proteomics identifies NCOA4 as the cargo receptor mediating ferritinophagy. *Nature* **509**, 105–109 (2014).
48. T. Imai *et al*., Intracellular Fe^{2+} accumulation in endothelial cells and pericytes induces blood-brain barrier dysfunction in secondary brain injury after brain hemorrhage. *Sci. Rep.* **9**, 6228 (2019).
49. N. Ohashi, A. Unver, N. Zhi, Y. Rikihisa, Cloning and characterization of multigenes encoding the immunodominant 30-kilodalton major outer membrane proteins of *Ehrlichia canis* and application of the recombinant protein for serodiagnosis. *J. Clin. Microbiol.* **36**, 2671–2680 (1998).
50. D. J. Lane *et al*., Cellular iron uptake, trafficking and metabolism: Key molecules and mechanisms and their roles in disease. *Biochim. Biophys. Acta* **1853**, 1130–1144 (2015).
51. M. Tang, Z. Chen, D. Wu, L. Chen, Ferritinophagy/ferroptosis: Iron-related newcomers in human diseases. *J. Cell. Physiol.* **233**, 9179–9190 (2018).
52. N. Ohashi, N. Zhi, Q. Lin, Y. Rikihisa, Characterization and transcriptional analysis of gene clusters for a type IV secretion machinery in human granulocytic and monocytic ehrlichiosis agents. *Infect. Immun.* **70**, 2128–2138 (2002).
53. Z. Cheng, X. Wang, Y. Rikihisa, Regulation of type IV secretion apparatus genes during *Ehrlichia chaffeensis* intracellular development by a previously unidentified protein. *J. Bacteriol.* **190**, 2096–2105 (2008).
54. J. S. Armstrong, M. Whiteman, Measurement of reactive oxygen species in cells and mitochondria. *Methods Cell Biol.* **80**, 355–377 (2007).
55. Y. Rikihisa, Subversion of RAB5-regulated autophagy by the intracellular pathogen *Ehrlichia chaffeensis*. *Small GTPases* **10**, 343–349 (2017).
56. C. Wandersman, P. Delepelaire, Bacterial iron sources: From siderophores to hemophores. *Annu. Rev. Microbiol.* **58**, 611–647 (2004).
57. M. Miethke, M. A. Marahiel, Siderophore-based iron acquisition and pathogen control. *Microbiol. Mol. Biol. Rev.* **71**, 413–451 (2007).
58. J. B. Neilands, Siderophores: Structure and function of microbial iron transport compounds. *J. Biol. Chem.* **270**, 26723–26726 (1995).
59. R. M. Roop *et al*., "Metal acquisition by Brucella strains" in *Brucella: Molecular Microbiology and Genomics*, I. López-Goñi, D. O'Callaghan, Eds. (Caister Academic, 2012), pp. 179–199.
60. J. Lechowicz, A. Krawczyk-Balska, An update on the transport and metabolism of iron in Listeria monocytogenes: The role of proteins involved in pathogenicity. *Biometals* **28**, 587–603 (2015).
61. Y. Wei, E. R. Murphy, Shigella iron acquisition systems and their regulation. *Front. Cell. Infect. Microbiol.* **6**, 18 (2016).
62. B. H. Kvitko, A. Goodyear, K. L. Propst, S. W. Dow, H. P. Schweizer, *Burkholderia pseudomallei* known siderophores and hemin uptake are dispensable for lethal murine melioidosis. *PLoS Negl. Trop. Dis.* **6**, e1715 (2012).
63. N. P. Cianciotto, An update on iron acquisition by *Legionella pneumophila*: New pathways for siderophore uptake and ferric iron reduction. *Future Microbiol.* **10**, 841–851 (2015).
64. N. D. Pokorzynski, C. C. Thompson, R. A. Carabeo, Ironing out the unconventional mechanisms of iron acquisition and gene regulation in *Chlamydia*. *Front. Cell. Infect. Microbiol.* **7**, 394 (2017).
65. R. Faris *et al*., *Chlamydia trachomatis* CT229 subverts Rab GTPase-dependent CCV trafficking pathways to promote chlamydial infection. *Cell Rep.* **26**, 3380–3390.e5 (2019).
66. S. E. Sanchez, A. Omsland, Critical role for molecular iron in *Coxiella burnetii* replication and viability. *mSphere* **5**, e00458-20 (2020).
67. J. E. Cassat, E. P. Skaar, Iron in infection and immunity. *Cell Host Microbe* **13**, 509–519 (2013).
68. T. Kurz, J. W. Eaton, U. T. Brunk, The role of lysosomes in iron metabolism and recycling. *Int. J. Biochem. Cell Biol.* **43**, 1686–1697 (2011).
69. A. Terman, T. Kurz, Lysosomal iron, iron chelation, and cell death. *Antioxid. Redox Signal.* **18**, 888–898 (2013).
70. D. C. Radisky, J. Kaplan, Iron in cytosolic ferritin can be recycled through lysosomal degradation in human fibroblasts. *Biochem. J.* **336**, 201–205 (1998).
71. Y. Zhang *et al*., Lysosomal proteolysis is the primary degradation pathway for cytosolic ferritin and cytosolic ferritin degradation is necessary for iron exit. *Antioxid. Redox Signal.* **13**, 999–1009 (2010).
72. T. Asano *et al*., Distinct mechanisms of ferritin delivery to lysosomes in iron-depleted and iron-replete cells. *Mol. Cell. Biol.* **31**, 2040–2052 (2011).
73. K. A. Bauckman, E. Haller, I. Flores, M. Nanjundan, Iron modulates cell survival in a Ras- and MAPK-dependent manner in ovarian cells. *Cell Death Dis.* **4**, e592 (2013).
74. I. De Domenico, D. M. Ward, J. Kaplan, Autophagy, ferritin and iron chelation. *Autophagy* **6**, 157 (2010).
75. J. E. Dawson *et al*., Isolation and characterization of an *Ehrlichia* sp. from a patient diagnosed with human ehrlichiosis. *J. Clin. Microbiol.* **29**, 2741–2745 (1991).
76. R. F. Felsheim *et al*., Transformation of *Anaplasma phagocytophilum*. *BMC Biotechnol.* **6**, 42 (2006).